ISSN 0915-633X

NATIONAL INSTITUTE FOR FUSION SCIENCE

One Dimensional Simulation on Stability of Detached Plasma in a Tokamak Divertor

S. Nakazawa, N. Nakajima, M. Okamoto and N. Ohyabu

(Received - May 20, 1999)

NIFS-598 June 1999

RESEARCH REPORT
NIFS Series

NAGOYA, JAPAN

One Dimensional Simulation on Stability of Detached Plasma in a Tokamak Divertor

Shinji NAKAZAWA, Noriyoshi NAKAJIMA, Masao OKAMOTO, and Nobuyoshi OHYABU

National Institute for Fusion Science, Oroshi 322-6, Toki, Gifu 509-5292, Japan

The stability of radiation front in the Scrape-Off-Layer (SOL) of a tokamak is studied with a one dimensional fluid code; the time-dependent transport equations are solved in the direction parallel to a magnetic field line. The simulation results show that stable detached solutions exist, where the plasma temperature near the divertor target is $\sim$ 2eV. It is found that whenever such stable detached states are attained, the strong radiation front is contact with or at a small distance from the divertor target. When the energy externally injected into the SOL is decreased below a critical value, the radiation front starts to move towards the X-point, cooling the SOL plasma. In such cases, no stationary solutions such that the radiation front rests in the divertor channel are observed in our parameter space. This qualitatively corresponds to the results of tokamak divertor experiments which show the movement of radiation front.

KEYWORDS: detached plasma, radiation front, divertor, tokamak

§1. Introduction

In the next generation fusion reactors, it is one of the most important issue to reduce the heat load onto the divertor target. As a method to reduce the heat load to technically feasible level ($\sim 5\mathrm{MW/m^2}$), the detached divertor was proposed, and it has been intensively studied by theories,[1-3] simulations,[3-5] and experiments. [2] [6-9]

When the edge plasma is detached from the divertor target, the particle and heat fluxes decrease strongly, and the plasma pressure drops significantly along the magnetic field line in the divertor region. Hence, the detached plasma is considered to be an important candidate for reducing the heat load on the divertor target. Such an edge plasma condition has been demonstrated experimentally in a number of tokamaks, like JT-60U, Alcator C-Mod, and Doublet III.[6-9]

The experimental observations, however, show that the location of detachment front (or radiation front) is unstable. For example, it was observed in the Doublet III divertor that when the edge plasma near the divertor target starts a transition from an attached state to a detached one, the cold and dense plasma near the target flows into the SOL region surrounding the core plasma. As a result of this influx, the SOL plasma is cooled and small disruptions occur.[9] This characteristic is, of course, considered to be a disadvantage for the core plasma confinement. This result implicitly indicates that it is not easy to use a detached plasma from the view point of thermal stability of the front.

On the other hand, simulations on divertor plasmas, in which the various atomic processes are important, have been done by many authors. [3-5] In most cases, the stationary states of SOL plasma are treated, and as for the dynamical behaviors of plasma detachment, little work has been done.

The purpose of this paper is to present the results obtained from a one-dimensional fluid simulation on the detached plasma in a tokamak SOL. In particular, this simulation study is focused on the problem of whether the location of detachment front is stable or not.

This paper consists of four sections. In sec.2, the simulation model is described. In sec.3, the numerical simulation is performed. It is shown how the edge plasma changes from an attached state to a detached state as the heat injected into the system is decreased. Sec.4 gives our summary.

§2. Simulation Model

2.1 Plasma fluid equations

We apply a one-dimensional model to the divertor plasma. This model uses a simplfied geometry, and it treats a region between the midplane and the divertor target, as illustrated in Fig. 1.

Let us consider the hydrogen plasma. In order to simplify our analyses, we assume the charge neutrality and ambipolar condition, i.e. , $n_e = n_i = n$ and $v_e = v_i = v$, where n_e (n_i) is the electron (ion) density; v_e (v_i) the electron (ion) velocity parallel to the magnetic field line. In addition, we assume that the ion temperature T_i is equal to the electron temperature T_e. We can thus regard the SOL plasma as a single-fluid with density n, velocity v, and temperature T.

By denoting the coordinate along the magnetic field line by x, the one-dimensional transport equations are given as follows:[10]

continuity:

$$\frac{\partial n}{\partial t} + \frac{\partial (nv)}{\partial x} = s_n, \tag{2.1}$$

momentum:

$$\frac{\partial (mnv)}{\partial t} + \frac{\partial (mnv^2 + P)}{\partial x} = s_v, \tag{2.2}$$

energy:

$$\frac{\partial}{\partial t}(3nT+\frac{1}{2}mnv^2)+\frac{\partial}{\partial x}(5nTv+\frac{1}{2}mnv^3-\kappa^e{}_{\|}\frac{\partial T}{\partial x})=Q. \quad (2.3)$$

Here, the plasma pressure P is related to the density n and the temperature T through $P=2nT$; $\kappa^e{}_{\|}$ is the electron heat conductivity parallel to a field line of magnetic field; s_n, s_v, and Q are the particle, momentum, and energy source, respectively. These sources are defined as follows:

particle source:

$$s_n = nn_n\langle\sigma v\rangle_{ion}-n^2(\langle\sigma v\rangle_{rre}+\langle\sigma v\rangle_{3re}), \quad (2.4)$$

where n_n is the density of neutrals (hydrogenic atoms); $\langle\sigma v\rangle_{ion}$, $\langle\sigma v\rangle_{rre}$, and $\langle\sigma v\rangle_{3re}$ are the ionization,[11] radiative[12] and three-body recombination[13] rate coefficient, respectively.

momentum source:

$$s_v=-mnv\{n_n\langle\sigma v\rangle_{cex}+n(\langle\sigma v\rangle_{rre}+\langle\sigma v\rangle_{3re})\} \quad (2.5)$$

where $\langle\sigma v\rangle_{cex}$ is the charge exchange rate coefficient.[11]

energy source:

$$\begin{aligned}Q &= W_\perp h(x-a)\\ &-\left(\frac{1}{2}mv^2+3T\right)n^2(\langle\sigma v\rangle_{rre}+\langle\sigma v\rangle_{3re})\\ &-\left(\frac{1}{2}mv^2+\frac{3}{2}T\right)nn_n\langle\sigma v\rangle_{cex}\\ &-\varepsilon_{ion}nn_n\langle\sigma v\rangle_{ion}-W_{imp}. \end{aligned} \quad (2.6)$$

Here, the constant $W_\perp$ is the heat which is externally injected into the system. The function $h(x-a)$ is a step function: $h(x-a)=0$ for $x>a$ and $h(x-a)=1$ for $x<a$. In other words, the heat source is uniformly distributed in the region from the midplane (at $x=0$) to the X-point (at $x=a$). The constant ε_{ion} is the electron energy loss due to the ionization and excitation ($\varepsilon_{ion}=30$eV). The last term W_{imp} is the radiation cooling rate of impurity ions. In Fig. 2, the rate coefficients of atomic processes included in this simulation model are shown as a function of T. The curve of three-body recombination rate coefficient is for the plasma density of $1.0\times10^{19}m^{-3}$.

The models for neutrals and impurity ions will be discussed later.

2.2 *Boundary conditions*

As shown in Fig. 1, the computational domain contains two boundaries: the surface of the divertor target (at $x=L$) and the midplane (at $x=0$). At the divertor target, we have imposed the Bohm condition for the plasma velocity:

$$v_d=\sqrt{\frac{2T_d}{m}}, \quad (2.7)$$

i.e, the plasma fluid flows into the target with the sound velocity, where the subscript d denotes the quantities at the surface of the divertor target (Throughout this paper, this notation will be used).

Also, the heat flux to the target is prescribed as

$$5n_dT_dv_d+\frac{1}{2}mn_dv_d{}^3-\left(\kappa^e{}_{\|}\frac{\partial T}{\partial x}\right)_d=\gamma n_dT_dv_d, \quad (2.8)$$

where γ is the sheath energy transmission factor. According to the sheath theory,[14] if no secondary electron at the target is considered, γ is given by

$$\gamma=\frac{2T_i}{T_e}+2+\frac{1}{2}\ln\left(\frac{m_i/m_e}{2\pi(1+T_i/T_e)}\right). \quad (2.9)$$

In our cases for hydrogen plasma with $T_e=T_i$, the factor γ is approximately 6.5.

At the midplane, assuming the symmetry with respect to the midplane, we have employed the following conditions:

$$\frac{\partial n}{\partial x}=0, \quad (2.10)$$

$$\frac{\partial T}{\partial x}=0, \quad (2.11)$$

$$v=0. \quad (2.12)$$

2.3 *Neutral gas model*

We evaluate the neutral density n_n by using a diffusion model. In this model, it is assumed that the neutrals, which are emitted from the wall, are diffusing across the background plasma through charge exchange process. Then, the neutral flux is decreased by ionization and increased by recombination process. The diffusion equation for neutral density is given by

$$\begin{aligned}\frac{\partial n_n}{\partial t}-\frac{\partial}{\partial z}\left(D\frac{\partial n_n}{\partial z}\right) &= -nn_n\langle\sigma v\rangle_{ion}\\ &+n^2(\langle\sigma v\rangle_{rre}+\langle\sigma v\rangle_{3re}),\end{aligned} \quad (2.13)$$

where z is the length of magnetic field line projected onto the poloidal plane, as shown in Fig. 3. The relation between the length z and the coordinate x along the field line is given by $dz=dx\sin\theta$, where θ is the angle at which a magnetic field line intersects the divertor target. The diffusion coefficient D due to the charge exchange is

$$D=\frac{T}{mn\langle\sigma v\rangle_{cex}}. \quad (2.14)$$

The equation (2.13) requires the the boundary condition. At the divertor target, we adopt the condition

$$\left(D\frac{\partial n_n}{\partial z}\right)_d=-n_dv_d\sin\theta, \quad (2.15)$$

that is, the z component of neutral flux is set to be equal to that of plasma flux. (This physical meaning is that 100 percent recycling at the wall is assumed). Using the continuity equation (2.1), the diffusion equation (2.13), and the above boundary condition (2.15), we can easily confirm that the condition (2.15) also guarantees the conservation of the total particle number in the system: $\int_0^L(n+n_n)\,dx=const.$. This gives a realistic boundary condition. In fact, when the SOL plasma becomes unsta-

ble, the detachement front can move rapidly (The time scale of this transport can be of the order of $\sim$ 1msec) In this case we should assume that the sum of plasma particle number in the SOL and neutral particle number in the SOL is conserved.

2.4 Impurity model

The coronal model is used to compute the energy loss due to the impurity radiation W_{imp}, which is given by

$$W_{imp} = nn_I L(T), \tag{2.16}$$

where n_I is the density of impurity ions, $L(T)$ is the impurity cooling rate and depends only on the plasma temperature.[15] Carbon is the only impurity species considered in our simulations. The density n_I is given by using a fixed fraction model:

$$n_I = \xi n, \tag{2.17}$$

where the constant ξ is the impurity fraction. In Fig. 2, the cooling rate $L(T)$ for carbon is shown as a function of T.

§3. Simulation Results

Using the fluid model described in the previous section, we carry out numerical simulations. A semi-implicit method is employed to carry out the time integration; Only diffusion parts are solved using implicit scheme and the others are explicitly solved with the Runge-Kutta scheme. Fixed simulation parameters are as follows: The system length is $L = 50$m; The distance between the midplane and the X-point is $a = 35$m; Carbon is the only impurity species, and its fraction is $\xi = 0.05$; The field line intersects the target at an angle $\theta = 5.0°$. By carrying out the simulations with different values of heat source $W_\perp$, the change in plasma parameters are observed from the attached states to the dettached states. The values of $W_\perp$ scanned in simulations are in the range $1.0 < W_\perp < 2.2\mathrm{MW/m^3}$.

In our simulation code, all lengths and velocities are normalized to the system length L and the velocity v_{T0}, respectively, where v_{T0} is ion thermal velocity given by $v_{T0} = \sqrt{T_0/\mathrm{m}}$, and where $T_0 = 10$eV. The total grid number is 2048. The grid spacing is $\Delta \simeq 0.48 \times 10^{-3}$. The time step is $\delta t = 1.0 \times 10^{-5}$. The Courant-number is $c\delta t/\Delta x \sim 0.02$, where c is the typical plasma flow velocity.

Before giving the simulation results, let us evaluate the size of the total energy externally injected into the system. For the case of a tokamak with the major radius R and the SOL width d, the energy flowing into the SOL region would be estimated by $Q_{total} \sim 2\pi R d W_\perp 2a\theta$. Using typical tokamak values of $R = 3$m, $d = 2 \times 10^{-2}$m, and simulation parameters of $W_\perp = 1.0\mathrm{MW/m^3}$,$\theta = 5.0°$, $a = 35$m, we obtain $Q_{total} \sim 2.3$MW, which will be a reasonable value as tokamak parameter.

First, we show stationary solutions for an attached case with $W_\perp = 2.0\mathrm{MW/m^3}$ in Fig. 4. In the figure, the midplane is at $x = 0$, and the divertor target is at $x = 50$m. The vertical dotted line at $x = 35$m represents the X-point where the heat source distribution ends. Figure 4 (d) shows that neutrals are localized at the target, and so the particle sources due to ionization also localized at the same point (Fig. 4(f)). The edge temperature is at around 15eV, at which the impurity radiation and recombination is not large, so that the dominant process of energy loss is the ionization (Fig. 4(h)). This causes a rapid fall in the energy flux near the target (Fig. 4(g)).

Figure 5 shows profiles of plasma parameters for a detached case with $W_\perp = 1.3\mathrm{MW/m^3}$. In comparison with the attached case, the edge plasma with the lower temperature can be obtained; the edge temperature is observed to be $\sim$ 2eV. The energy loss due to the impurity radiation is comparable to that of ionization and charge exchange (Fig. 5 (h)). The x position at which impurity radiation, charge exchange, and ionization phenomena takes place are superposed at nearly the same location. The energy flux rapidly decreases to around 10% of input power as one move to the divertor target (Fig. 5(g)).

The detached cases are different from the attached cases in that the impurity radiation region exists near the target. For all the detached cases where the solution is in stationary state, the impurity radiation region is contact with or very close to the target; the x position of the peak is $49 < x < 50$m.

As previously mentioned, parameter scans are carried out with the various values of input power $W_\perp$. In the range of $1.3 < W_\perp < 2.2\mathrm{MW/m^3}$, we can obtain stationary solutions. However, for lower values of the heat source ($W_\perp < 1.3\mathrm{MW/m^3}$), the detachement front becomes unstable and the stationary solution is no longer observed.

We show such an example in Fig. 6. This figure shows the time evolution of profiles of density n and temperature T for the case with $W_\perp = 1.2\mathrm{MW/m^3}$. Here, as the initial profile, we put a stationary solution of the detached plasma with $W_\perp = 1.3\mathrm{MW/m^3}$. It is found that both the density and the temperature profile are moving nearly steadily from the target to the X-point, extending a region of cold and tenuous plasma.

Figure 7 shows snapshots at $t = 4.75$ms of moving detachment front for various plasma parameters. A low-density and low-temperature region is in the range $43 < x < 50$m (Fig. 7(a) (b)). The density falls sharply at $x = 43$m. At this time, the temperature in front of the target is observed to be $\sim 0.1 - 1.0$eV. Fig. 7(f) shows that the recombination is occurring at the detachment front. Expanded views of several energy loss rates are shown in Fig. 7(h). In this figure, the value of energy loss for each atomic process is given in parentheses. The sum of the energy losses (Total energy loss) is $\sim 51\mathrm{MW/m^2}$ and this value is larger than total injection power of $42\mathrm{MW/m^2}$.

The dependences of edge density n_d, edge temperature T_d, and energy loss rates for various atomic processes, on the total injection power W_{in} are shown in Fig. 8, where W_{in} is given as $W_{in} = W_\perp a$. As W_{in} is decreased from $78MW/m^2$ to $65MW/m^2$, the temperature T_d falls

from 20eV to around 10eV. Then, the impurity radiation loss W_{imp} increases rapidly and it causes a steep drop in T_d of 10eV at $W_{in} \sim 62MW/m^2$. It is found that the cold and dense plasmas with a strong impurity radiation are produced near the divertor target in the parameter range $42 < W_{in} < 60\mathrm{MW/m^2}$, while the ratio of energy flux at the target to injection energy W_{in}, $\gamma nTv/W_{in}$, is substantially decreased to below 10%. In the figures, such plasmas are designated by a word 'detached'. In the cases with $W_{in} < 42\mathrm{MW/m^2}$, it is observed that the detachment front moves to upstream region, and then stationary solutions are not obtained.

§4. Summary

We have studied the stability of detachment front in a tokamak divertor with a one dimensional fluid code.

First, we have presented the simulation model; The plasma fluid is described with the time-dependent transport equations based on the single-fluid theory, where ionization, charge exchange, and recombination effects are taken into account in those equations. They are solved in the direction parallel to a magnetic field line. The neutral gas is approximately treated by using a diffusion model. The fixed fraction model and the coronal approximation are used to give the impurity density and radiation loss.

Next, we have carried out numerical simulations. The simulation results show that when detached stationary solutions are observed, the heat flux onto the target is significantly decreased to around 10% of the input power. However, whenever such detached states are attained, the strong radiation front is in contact with or at a small distance from the divertor target. Probably, such a condition will not be favorable, because the target will be subjected to an amount of radiation (about one-half of total radiation power). When the input power is decreased below a critical value in magnitude, the radiation front moves towards the X-point, cooling the SOL plasma. For such cases, no staionary solutions are observed. This result implicitly indicates that it is not easy to use a detached plasma from the view point of the location-stability of detachment front.

In our discussions, there is one point we should note. We have carried out simulations using one-dimensional model. However, in a actual tokamak SOL, two-dimensional effects are important. For instance, if we consider the cases where the SOL plasma is detached from the inner section of the target, while the plasma attaches to the outer section of the target (what is called 'partial detachment'), we have to treat a two-dimensional model to discuss the stability of detachment front. Therefore, there is a doubt whether our one-dimensional interpretations on the detachment front is directly applicable to the actual problem. It seems that our results is valid only for the cases of 'full detachment'.

In this paper we have ignored the transports for impurity species. If we consider those transports, our simulation results will be modified. For example, since the thermal force between the plasma fluid and impurity ions proportional to the temperature gradient have an effect on pushing the impurity ions to the core, the force will probably lead to further destabilization of detachment front. This problem will be discussed elsewhere.

Acknowledgements

One of the authors (S.Nakazawa) wish to acknowledge Dr.Ishizaki and Dr.Orito for their fruitful discussions.

1) K. Miyamoto and N. Asakura: J. Phys. Soc. Jpn **74**, No.3 (1998), pp.266-273
2) C. S. Pitcher and P. C. Stangeby, Plasma Phys. Control. Fusion **39**, (1997) 779-930.
3) R. Goswami, P. K. Kaw, M. Warrier, R. Singh, S. P. Deshpande in Proceedings of the 17th IAEA Fusion Energy Conference (International Atomic Energy Agency, Yokohama, Japan, 19-24 October (1998).
4) Gary D. Porter, et al.: Phys. Plasmas **3** (5), (1996) 1967.
5) E. L. Vold, F. Najmabadi, and R. W. Conn: J. Com. Phys. **103**, (1992) pp.300-319
6) M. Nagami, JT-60 Team : J. Nucl. Materials. **2**, (1995) 220-222.
7) J. A. Goetz, et al. : Phys. Plasmas **3** (5), (1996) 1908.
8) M. E. Fenstermacher, et al. : J. Nucl. Materials **241-243**, (1997) 666.
9) N. Ohyabu , et al. : GA-Report, GA-A16484, (1982)
10) S. I. Braginskii: in *Reviews of Plasma Physics*, ed. M A. Leontovich (Consultants Bureau. New York, 1965), Vol.1, pp.205-311.
11) R. Freeman and E. Jones, CLM-R-137, Culham Laboratory. Abingdon (1974)
12) Yu. Gordeev, et al. : Pisma Zh. Eksperim. Theor. Fiz. **25**, (1977) 223.
13) E. Hinnov and J. G. Hirshberg, Phys. Rev., **125**, (1962) 795
14) J. Wesson: *Tokamaks*, Clarendon Press, Oxford (1997)
15) D. E. Post and R. V. Jensen: Atomic Data and Nuclear Data Tables **20**, (1977) 397.

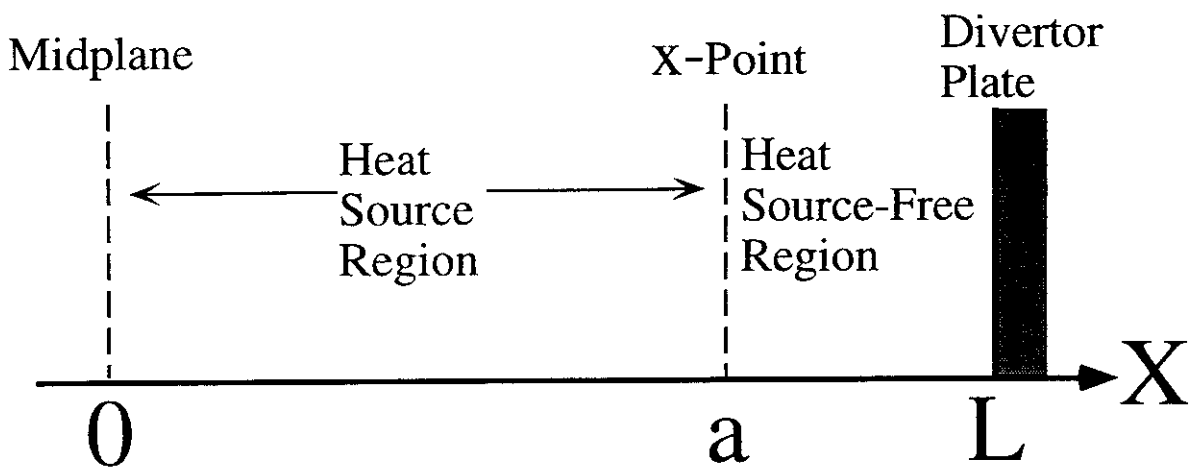

Fig.1 Schematic of one-dimensional simulation model

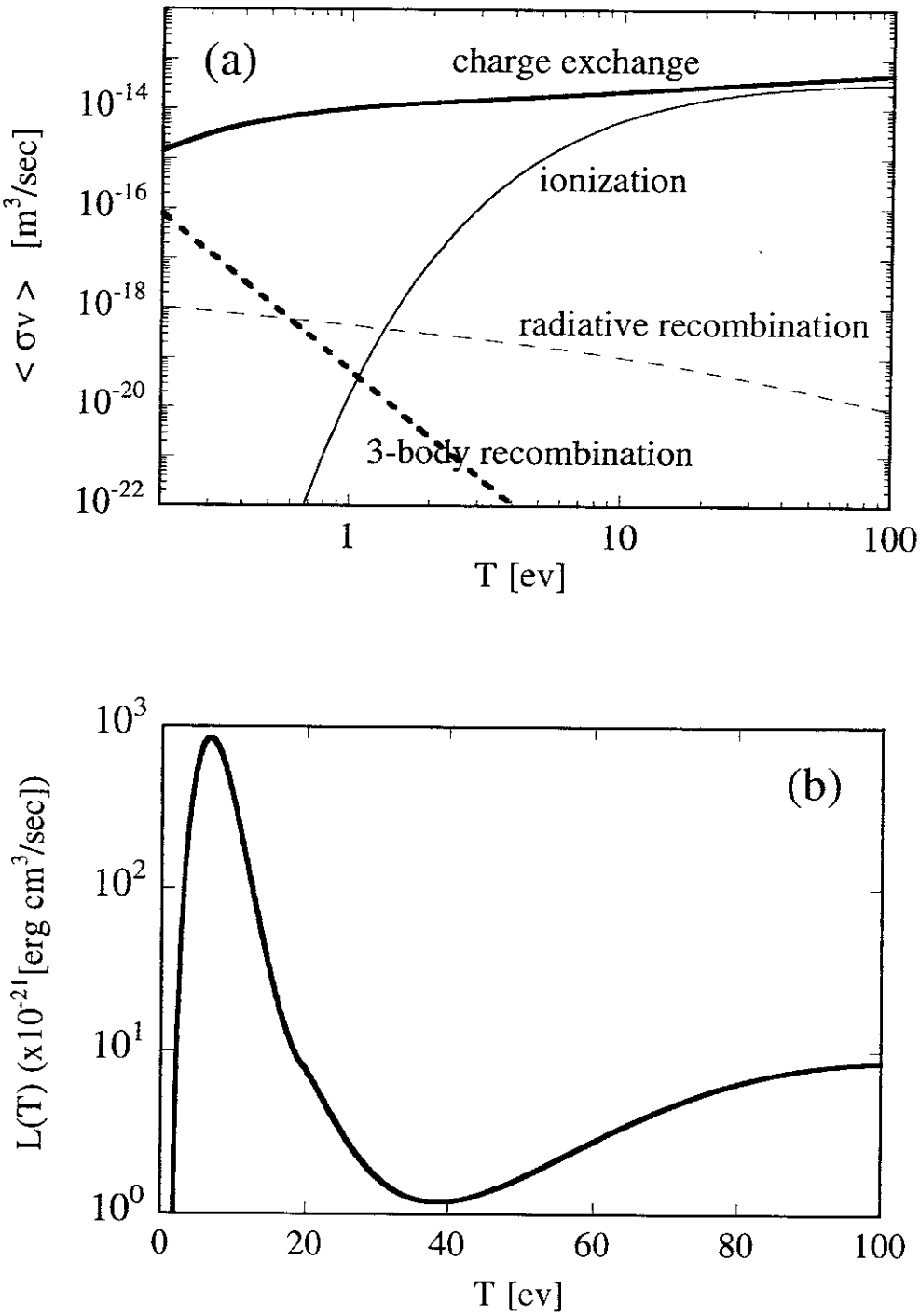

Fig.2 Rate coefficients of various atomic processes for atomic hydrogen when the plasma density is $n=1.0 \times 10^{19}$ m^{-3} (a). Cooling rate for carbon (b).

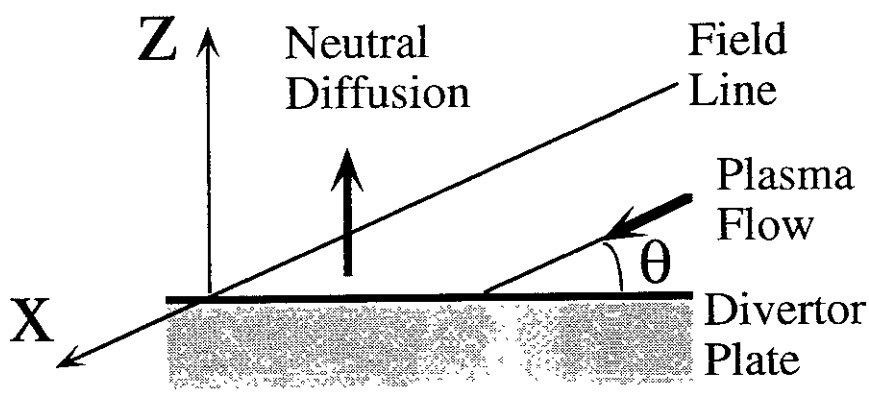

Fig.3 The relation between the length z and the coodinate x along the field line.

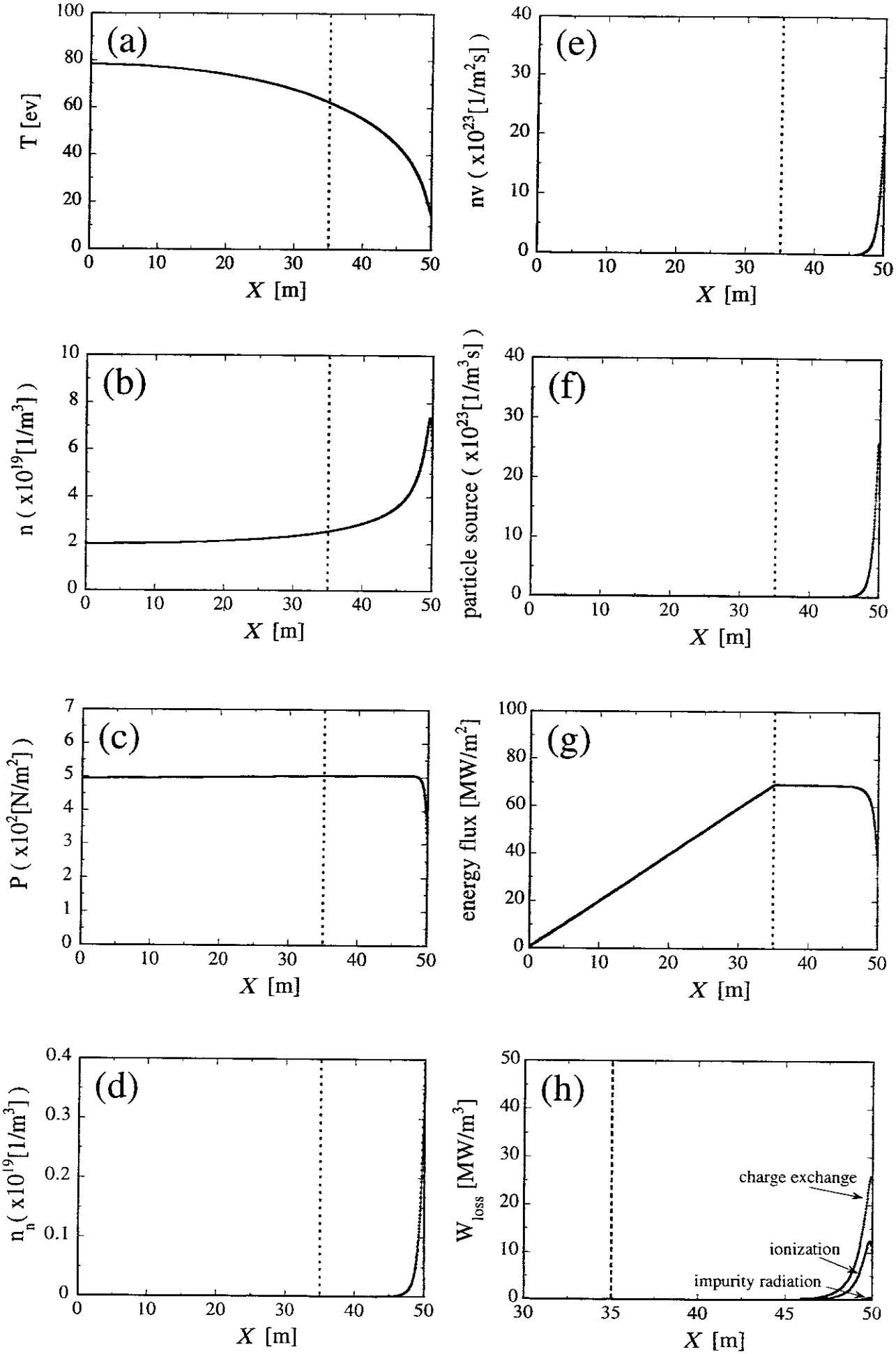

Fig.4 Plots of plasma parameters along the field line. Here, an attached case is shown.

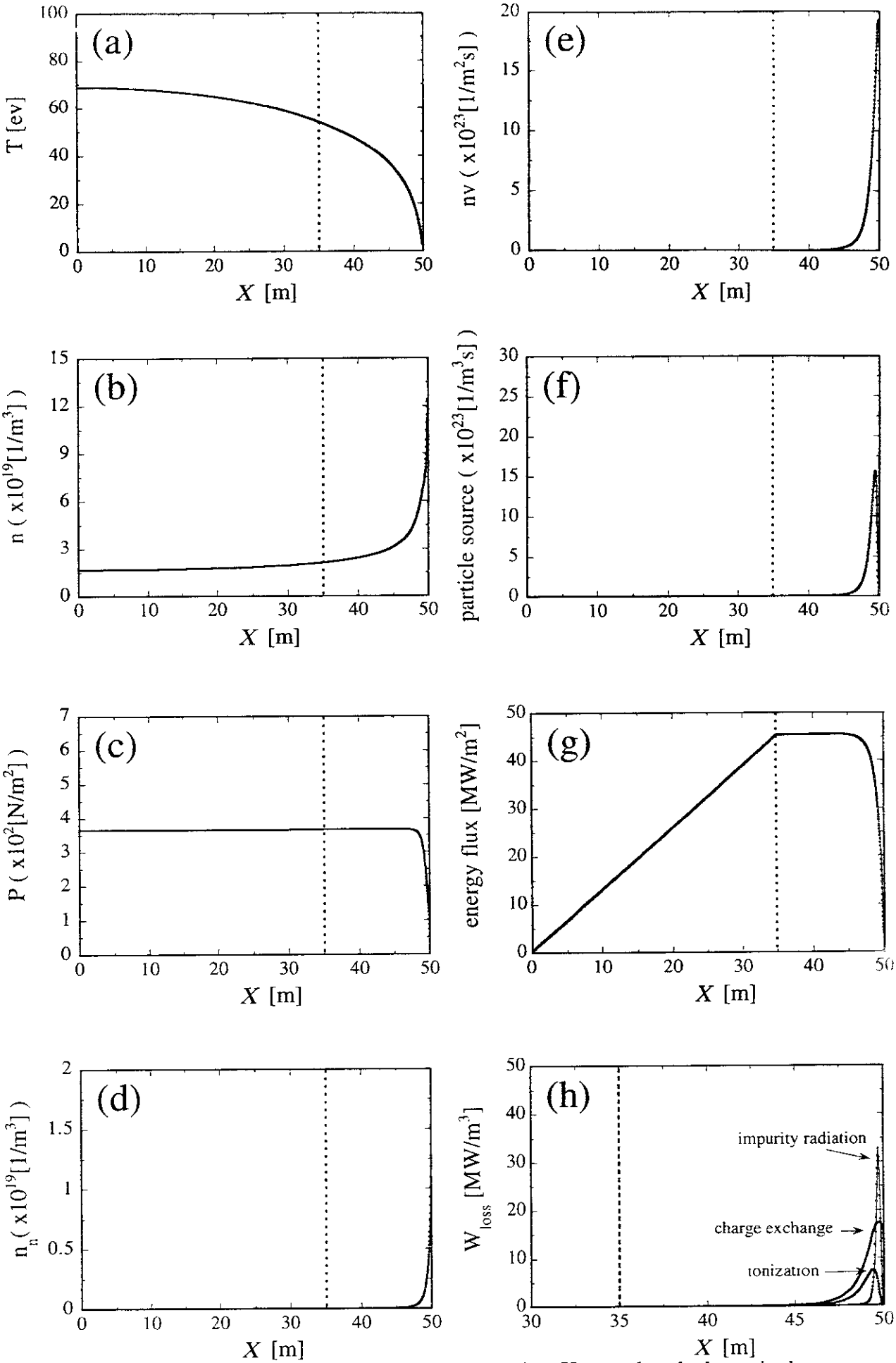

Fig.5 Plots of plasma parameters along the field line. Here, a detached case is shown.

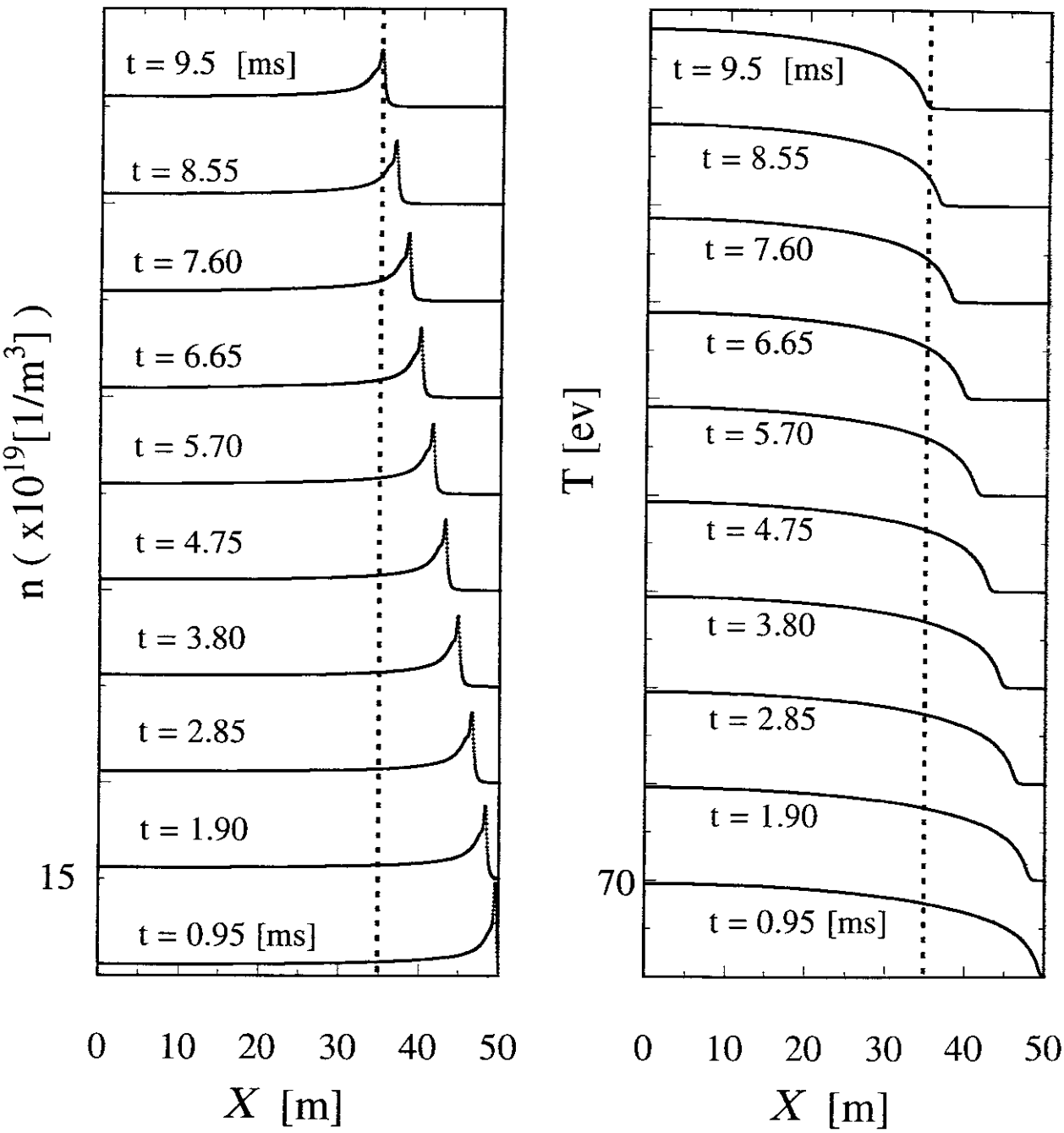

Fig.6 Density and temperature profiles of a detached plasma at various times.

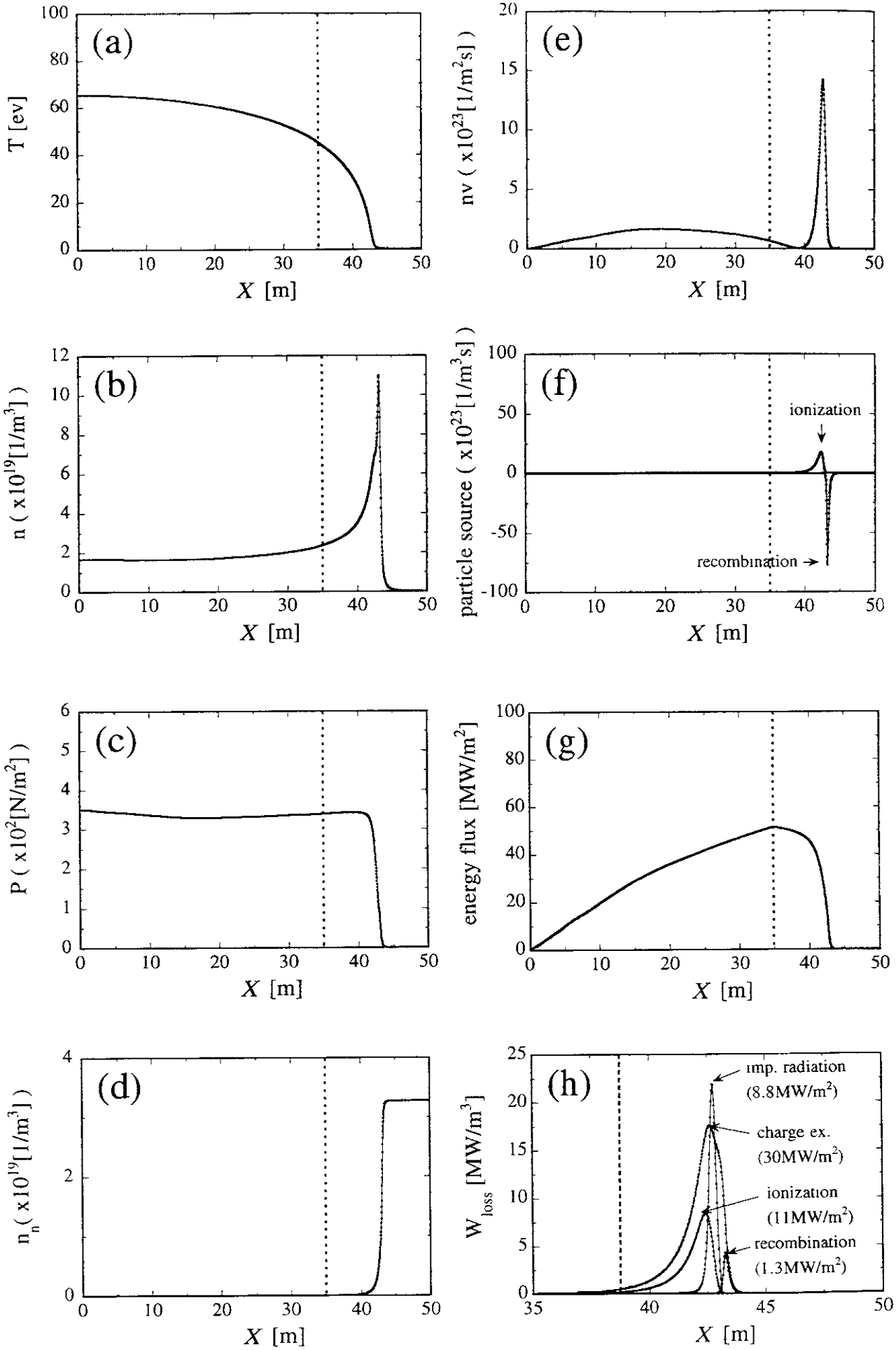

Fig.7 Snapshots of moving detachment front.

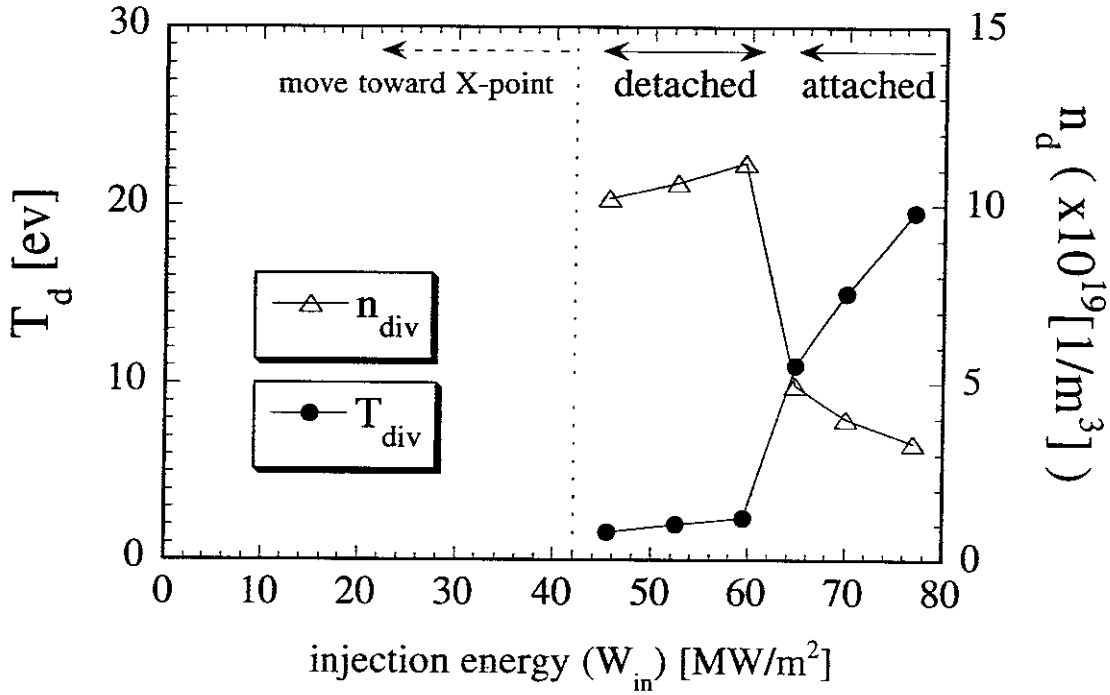

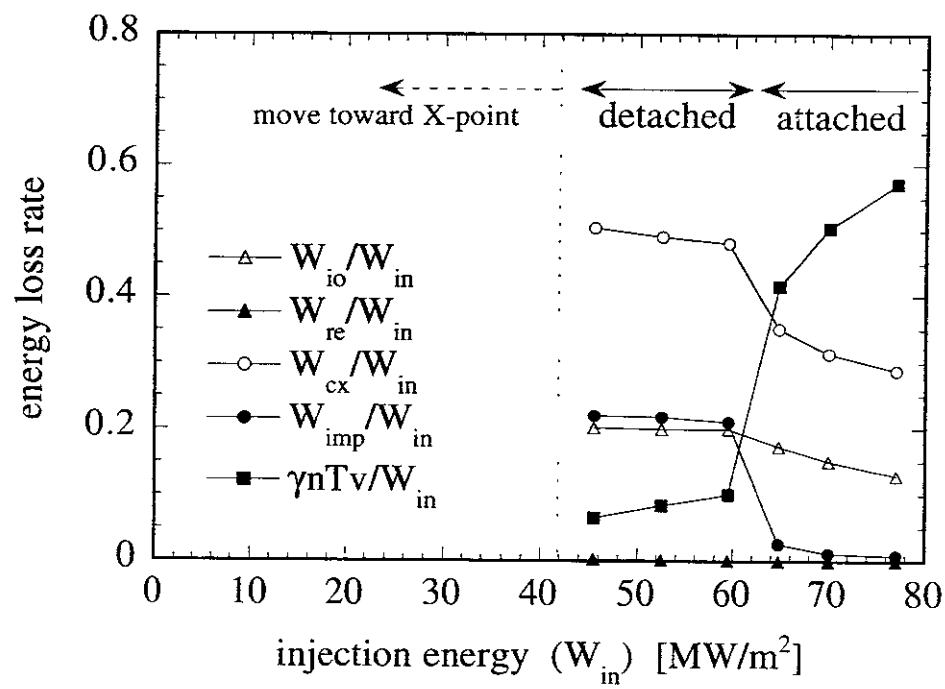

Fig.8 Dependences of n, T, and energy loss rates for various atomic processes on the injection power W_{in} .

Recent Issues of NIFS Series

NIFS-534 Y Matsukawa T Suda, S Ohnuki and C Namba,
Microstructure and Mechanical Property of Neutron Irradiated TiNi Shape Memory Alloy, Jan 1998

NIFS-535 A. Fujisawa H Iguchi H Idei, S Kubo, K Matsuoka, S Okamura, K Tanaka, T Minami, S Ohdachi, S Morita, H Zushi, S Lee, M Osakabe, R Akiyama, Y Yoshimura, K. Toi, H Sanuki, K Itoh, A Shimizu, S Takagi, A. Ejiri C Takahashi, M. Kojima, S Hidekuma, K Ida, S Nishimura, N Inoue, R Sakamoto, S -I. Itoh, Y Hamada M. Fujiwara,
Discovery of Electric Pulsation in a Toroidal Helical Plasma, Jan 1998

NIFS-536 Lj.R Hadzievski, M.M Skoric, M. Kono and T Sato
Simulation of Weak and Strong Langmuir Collapse Regimes, Jan 1998

NIFS-537 H Sugama, W Horton
Nonlinear Electromagnetic Gyrokinetic Equation for Plasmas with Large Mean Flows Feb 1998

NIFS-538 H Iguchi, T P Crowley, A Fujisawa, S Lee, K. Tanaka, T Minami, S. Nishimura, K Ida, R Akiyama, Y. Hamada, H , Idei M Isobe, M. Kojima, S Kubo, S Morita, S Ohdachi, S Okamura, M Osakabe, K Matsuoka, C. Takahashi and K Toi,
Space Potential Fluctuations during MHD Activities in the Compact Helical System (CHS): Feb. 1998

NIFS-539 Takashi Yabe and Yan Zhang,
Effect of Ambient Gas on Three-Dimensional Breakup in Coronet Formation Process, Feb. 1998

NIFS-540 H Nakamura, K Ikeda and S. Yamaguchi
Transport Coefficients of InSb in a Strong Magnetic Field, Feb 1998

NIFS-541 J Uramoto,
Development of ν_μ Beam Detector and Large Area ν_μ Beam Source by H_2 Gas Discharge (I). Mar 1998

NIFS-542 J Uramoto,
Development of $bar{\nu}_\mu$ Beam Detector and Large Area $bar{\nu}_\mu$ Beam Source by H_2 Gas Discharge (II). Mar 1998

NIFS-543 J Uramoto,
Some Problems inside a Mass Analyzer for Pions Extracted from a H_2 Gas Discharge, Mar 1998

NIFS-544 J Uramoto,
Simplified ν_μ, $bar{\nu}_\mu$ Beam Detector and ν_μ, $bar{\nu}_\mu$ Beam Source by Interaction between an Electron Bunch and a Positive Ion Bunch: Mar 1998

NIFS-545 J Uramoto,
Various Neutrino Beams Generated by D_2 Gas Discharge: Mar 1998

NIFS-546 R Kanno, N Nakajima, T. Hayashi and M Okamoto,
Computational Study of Three Dimensional Equilibria with the Bootstrap Current, Mar 1998

NIFS-547 R Kanno, N Nakajima and M Okamoto,
Electron Heat Transport in a Self-Similar Structure of Magnetic Islands: Apr 1998

NIFS-548 J.E Rice,
Simulated Impurity Transport in LHD from MIST: May 1998

NIFS-549 M M Skoric, T Sato, A M Maluckov and M.S. Jovanovic
On Kinetic Complexity in a Three-Wave Interaction, June 1998

NIFS-550 S Goto and S Kida
Passive Scalar Spectrum in Isotropic Turbulence. Prediction by the Lagrangian Direct-interaction Approximation: June 1998

NIFS-551 T Kuroda, H Sugama R Kanno, M. Okamoto and W Horton,
Initial Value Problem of the Toroidal Ion Temperature Gradient Mode : June 1998

NIFS-552 T Mutoh, R Kumazawa, T Seki, F Simpo G Nomura, T. Ido and T Watari
Steady State Tests of High Voltage Ceramic Feedthoughs and Co-Axial Transmission Line of ICRF Heating System for the Large Helical Device : June 1998

NIFS-553 N. Noda. K. Tsuzuki, A Sagara. N Inoue, T. Muroga,
oronaization in Future Devices -Protecting Layer against Tritium and Energetic Neutrals-' July 1998

NIFS-554 S. Murakami and H. Saleem,
Electromagnetic Effects on Rippling Instability and Tokamak Edge Fluctuations July 1998

NIFS-555 H. Nakamura, K. Ikeda and S Yamaguchi,
Physical Model of Nernst Element; Aug 1998

NIFS-556 H Okumura, S. Yamaguchi, H Nakamura. K. Ikeda and K Sawada,
Numerical Computation of Thermoelectric and Thermomagnetic Effects Aug 1998

NIFS-557 Y. Takeiri, M Osakabe, K Tsumori, Y Oka, O Kaneko, E. Asano, T Kawamoto, R Akiyama and M. Tanaka,
Development of a High-Current Hydrogen-Negative Ion Source for LHD-NBI System, Aug.1998

NIFS-558 M. Tanaka, A. Yu Grosberg and T. Tanaka,
Molecular Dynamics of Structure Organization of Polyampholytes:Sep. 1998

NIFS-559 R Horiuchi, K. Nishimura and T. Watanabe,
Kinetic Stabilization of Tilt Disruption in Field-Reversed Configurations; Sep. 1998
(IAEA-CN-69/THP1/11)

NIFS-560 S. Sudo, K. Kholopenkov, K Matsuoka, S Okamura, C Takahashi, R. Akiyama. A Fujisawa, K Ida, H. Idei, H. Iguchi, M Isobe. S Kado, K. Kondo, S Kubo, H Kuramoto, T. Minami, S Morita, S Nishimura, M. Osakabe, M Sasao, B. Peterson, K. Tanaka, K. Toi and Y Yoshimura,
Particle Transport Study with Tracer-Encapsulated Solid Pellet Injection. Oct. 1998
(IAEA-CN-69/EXP1/18)

NIFS-561 A. Fujisawa, H. Iguchi, S Lee, K. Tanaka, T. Minami, Y. Yoshimura M Osakabe, K. Matsuoka, S. Okamura, H. Idei, S Kubo, S. Ohdachi, S. Morita, R. Akiyama, K. Toi, H. Sanuki, K Itoh, K. Ida. A. Shimizu, S. Takagi, C Takahashi, M Kojima. S Hidekuma, S. Nishimura, M Isobe, A. Ejiri, N Inoue, R. Sakamoto, Y Hamada and M Fujiwara,
Dynamic Behavior Associated with Electric Field Transitions in CHS Heliotron/Torsatron; Oct. 1998
(IAEA-CN-69/EX5/1)

NIFS-562 S Yoshikawa,
Next Generation Toroidal Devices; Oct. 1998

NIFS-563 Y. Todo and T Sato,
Kinetic-Magnetohydrodynamic Simulation Study of Fast Ions and Toroidal Alfvén Eigenmodes. Oct. 1998
(IAEA-CN-69/THP2/22)

NIFS-564 T. Watari, T. Shimozuma, Y Takeiri, R. Kumazawa, T. Mutoh, M. Sato, O Kaneko, K Ohkubo, S. Kubo, H. Idei, Y Oka, M. Osakabe, T. Seki, K. Tsumori, Y. Yoshimura, R. Akiyama, T. Kawamoto, S Kobayashi, F Shimpo, Y Takita, E Asano, S Itoh, G Nomura, T. Ido, M Hamabe, M. Fujiwara, A. Iiyoshi, S. Morimoto, T. Bigelow and Y.P. Zhao,
Steady State Heating Technology Development for LHD; Oct. 1998
(IAEA-CN-69/FTP/21)

NIFS-565 A. Sagara, K Y Watanabe, K. Yamazaki, O Motojima, M Fujiwara, O. Mitarai, S Imagawa, H. Yamanishi, H Chikaraishi, A. Kohyama, H. Matsui T Muroga, T Noda, N. Ohyabu, T Satow A.A. Shishkin, S. Tanaka T Terai and T Uda,
LHD-Type Compact Helical Reactors; Oct 1998
(IAEA-CN-69/FTP/03(R)

NIFS-566 N Nakajima, J Chen, K. Ichiguchi and M. Okamoto,
Global Mode Analysis of Ideal MHD Modes in L=2 Heliotron/Torsatron Systems. Oct 1998
(IAEA-CN-69/THP1/08)

NIFS-567 K. Ida, M. Osakabe K. Tanaka, T. Minami. S. Nishimura, S. Okamura, A. Fujisawa, Y. Yoshimura. S. Kubo, R. Akiyama. D.S.Darrow, H Idei, H. Iguchi, M. Isobe, S. Kado, T. Kondo, S Lee. K Matsuoka, S. Morita, I. Nomura, S. Ohdachi. M. Sasao, A. Shimizu, K. Tumori, S Takayama, M. Takechi, S Takagi, C. Takahashi, K. Toi and T. Watari,
Transition from L Mode to High Ion Temperature Mode in CHS Heliotron/Torsatron Plasmas, Oct 1998
(IAEA-CN-69/EX2/2)

NIFS-568 S. Okamura, K. Matsuoka, R. Akiyama, D.S. Darrow, A. Ejiri, A. Fujisawa, M. Fujiwara, M. Goto, K. Ida H. Idei, H. Iguchi, N. Inoue, M. Isobe, K. Itoh. S. Kado, K. Khlopenkov, T. Kondo, S. Kubo, A. Lazaros, S. Lee, G Matsunaga, T. Minami, S. Morita, S.

Murakami, N Nakajima, N Nikai, S Nishimura, I Nomura, S Ohdachi, K Ohkuni, M Osakabe, R Pavlichenko, B Peterson, R Sakamoto H Sanuki M Sasao A Shimizu Y Shirai, S Sudo, S Takagi C Takahashi S Takayama M Takechi K Tanaka, K Toi, K Yamazaki Y Yoshimura and T Watari,
Confinement Physics Study in a Small Low-Aspect-Ratio Helical Device CHS Oct 1998
(IAEA-CN-69/OV4/5)

NIFS-569 M M Skoric T Sato A Maluckov, M S Jovanovic
Micro- and Macro-scale Self-organization in a Dissipative Plasma Oct 1998

NIFS-570 T Hayashi, N Mizuguchi, T-H Watanabe T Sato and the Complexity Simulation Group
Nonlinear Simulations of Internal Reconnection Event in Spherical Tokamak Oct 1998
(IAEA-CN-69/TH3/3)

NIFS-571 A Iiyoshi, A Komori A Ejiri, M Emoto, H Funaba M Goto, K Ida, H Idei, S Inagaki, S Kado, O Kaneko, K Kawahata, S Kubo R Kumazawa, S Masuzaki, T Minami, J Miyazawa, T Morisaki, S. Morita, S Murakami., S Muto, T Muto, Y Nagayama, Y Nakamura, H Nakanishi, K Narihara, K Nishimura, N Noda, T Kobuchi, S Ohdachi, N Ohyabu, Y Oka, M Osakabe, T. Ozaki, B J. Peterson A Sagara, S Sakakibara, R Sakamoto, H Sasao, M Sasao, K Sato, M Sato, T Seki, T Shimozuma, M Shoji, H Suzuki, Y. Takeiri, K Tanaka, K Toi, T Tokuzawa, K Tsumori, I Yamada, H Yamada, S Yamaguchi, M Yokoyama, K.Y Watanabe, T Watari R Akiyama H Chikaraishi, K Haba S Hamaguchi S Iima, S Imagawa N Inoue, K Iwamoto, S Kitagawa, Y. Kubota, J Kodaira R. Maekawa, T. Mito T Nagasaka A Nishimura Y Takita, C Takahashi, K Takahata, K Yamauchi, H Tamura, T Tsuzuki, S Yamada, N Yanagi, H Yonezu, Y Hamada, K Matsuoka, K Murai, K Ohkubo, I Ohtake, M Okamoto, S Sato, T Satow, S Sudo, S. Tanahashi, K Yamazaki, M Fujiwara and O Motojima,
An Overview of the Large Helical Device Project. Oct. 1998
(IAEA-CN-69/OV1/4)

NIFS-572 M Fujiwara, H Yamada, A Ejiri M Emoto, H Funaba, M Goto, K Ida, H Idei, S Inagaki, S. Kado, O Kaneko, K Kawahata, A Komori, S. Kubo, R Kumazawa, S Masuzaki, T. Minami, J Miyazawa, T Morisaki, S Morita S Murakami, S Muto, T Muto, Y Nagayama, Y Nakamura. H. Nakanishi, K Narihara, K. Nishimura, N. Noda, T Kobuchi, S Ohdachi, N Ohyabu, Y. Oka, M. Osakabe, T Ozaki, B J. Peterson, A Sagara, S Sakakibara, R Sakamoto, H Sasao, M Sasao, K Sato, M Sato, T Seki, T Shimozuma, M Shoji, H Sazuki, Y Takeiri, K Tanaka, K Toi, T Tokuzawa, K Tsumori, I Yamada, S Yamaguchi, M Yokoyama, K Y Watanabe, T Watari, R Akiyama, H Chikaraishi, K Haba, S Hamaguchi M. Iima, S Imagawa, N Inoue, K. Iwamoto. S Kitagawa, Y Kubota J Kodaira, R Maekawa, T Mito, T Nagasaka, A Nishimura Y Takita, C Takahashi, K. Takahata, K Yamauchi, H Tamura T Tsuzuki S. Yamada, N Yanagi, H Yonezu, Y Hamada, K Matsuoka, K Murai, K Ohkubo, I Ohtake, M Okamoto, S Sato, T Satow, S Sudo, S Tanahashi, K Yamazaki, O Motojima and A Iiyoshi
Plasma Confinement Studies in LHD. Oct 1998
(IAEA-CN-69/EX2/3)

NIFS-573 O. Motojima, K. Akaishi, H Chikaraishi, H Funaba, S Hamaguchi, S. Imagawa, S Inagaki, N. Inoue, A Iwamoto, S. Kitagawa, A Komori, Y Kubota, R Maekawa, S Masuzaki, T. Mito J Miyazawa, T Morisaki, T Muroga, T. Nagasaka, Y Nakmura, A. Nishimura K Nishimura, N Noda, N Ohyabu, S Sagara, S Sakakibara, R. Sakamoto, S. Satoh, T Satow, M. Shoji, H. Suzuki, K. Takahata, H Tamura, K. Watanabe, H. Yamada, S. Yamada, S Yamaguchi, K. Yamazaki, N. Yanagi, T. Baba, H. Hayashi M Iima, T Inoue, S Kato, T Kato, T Kondo, S Moriuchi, H. Ogawa, I Ohtake, K. Ooba, H Sekiguchi, N Suzuki, S. Takami, Y Taniguchi, T Tsuzuki, N Yamamoto, K Yasui, H Yonezu M Fujiwara and A Iiyoshi,
Progress Summary of LHD Engineering Design and Construction Oct 1998
(IAEA-CN-69/FT2/1)

NIFS-574 K. Toi, M Takechi, S Takagi, G Matsunaga, M. Isobe, T Kondo, M Sasao, D S. Darrow, K. Ohkuni, S Ohdachi, R. Akiyama A Fujisawa, M. Gotoh, H Idei, K Ida, H. Iguchi, S Kado, M Kojima, S Kubo S Lee, K Matsuoka T Minami, S. Morita, N Nikai, S Nishimura, S Okamura, M Osakabe, A. Shimizu, Y Shirai, C Takahashi, K Tanaka, T Watari and Y Yoshimura,
Global MHD Modes Excited by Energetic Ions in Heliotron/Torsatron Plasmas, Oct 1998
(IAEA-CN-69/EXP1/19)

NIFS-575 Y. Hamada, A. Nishizawa Y Kawasumi, A Fujisawa, M. Kojima, K Narihara, K Ida, A. Ejiri, S Ohdachi, K Kawahata, K Toi, K Sato, T Seki, H Iguchi. K Adachi, S. Hidekuma, S.Hirokura, K Iwasaki T. Ido R Kumazawa. H Kuramoto, T. Minami, I. Nomura, M Sasao, K N. Sato, T. Tsuzuki, I Yamada and T Watari.
Potential Turbulence in Tokamak Plasmas. Oct 1998
(IAEA-CN-69/EXP2/14)

NIFS-576 S. Murakami, U Gasparino, H Idei, S Kubo, H Maassberg, N Marushchenko. N Nakajima. M. Romé and M Okamoto
5D Simulation Study of Suprathermal Electron Transport in Non-Axisymmetric Plasmas; Oct 1998
(IAEA-CN-69/THP1/01)

NIFS-577 S Fujiwara and T Sato,
Molecular Dynamics Simulation of Structure Formation of Short Chain Molecules, Nov. 1998

NIFS-578 T Yamagishi,
Eigenfunctions for Vlasov Equation in Multi-species Plasmas Nov 1998

NIFS-579 M Tanaka, A Yu Grosberg and T Tanaka,
Molecular Dynamics of Strongly-Coupled Multichain Coulomb Polymers in Pure and Salt Aqueous Solutions Nov 1998

NIFS-580 J. Chen, N Nakajima and M. Okamoto,
Global Mode Analysis of Ideal MHD Modes in a Heliotron/Torsatron System: I Mercier-unstable Equilibria, Dec. 1998

NIFS-581 M. Tanaka, A. Yu Grosberg and T Tanaka,
Comparison of Multichain Coulomb Polymers in Isolated and Periodic Systems: Molecular Dynamics Study: Jan. 1999

NIFS-582 V.S. Chan and S. Murakami
Self-Consistent Electric Field Effect on Electron Transport of ECH Plasmas, Feb 1999

NIFS-583 M. Yokoyama, N. Nakajima, M. Okamoto, Y. Nakamura and M. Wakatani,
Roles of Bumpy Field on Collisionless Particle Confinement in Helical-Axis Heliotrons: Feb. 1999

NIFS-584 T -H Watanabe, T Hayashi T Sato, M. Yamada and H. Ji
Modeling of Magnetic Island Formation in Magnetic Reconnection Experiment, Feb 1999

NIFS-585 R. Kumazawa, T Mutoh, T. Seki, F. Shinpo, G. Nomura, T. Ido, T. Watari, Jean-Marie Noterdaeme and Yangping Zhao
Liquid Stub Tuner for Ion Cyclotron Heating; Mar. 1999

NIFS-586 A. Sagara, M. Iima, S. Inagaki, N. Inoue, H Suzuki, K. Tsuzuki, S. Masuzaki, J. Miyazawa, S Morita, Y Nakamura, N. Noda, B. Peterson, S. Sakakibara, T. Shimozuma, H. Yamada, K. Akaishi, H. Chikaraishi, H Funaba O Kaneko, K. Kawahata A. Komori, N. Ohyabu, O Motojima, LHD Exp. Group 1, LHD Exp. Group 2,
Wall Conditioning at the Starting Phase of LHD: Mar 1999

NIFS-587 T. Nakamura and T Yabe,
Cubic Interpolated Propagation Scheme for Solving the Hyper-Dimensional Vlasov-Poisson Equation in Phase Space Mar 1999

NIFS-588 W X. Wnag, N. Nakajima, S Murakami and M Okamoto,
An Accurate δf Method for Neoclassical Transport Calculation; Mar. 1999

NIFS-589 K. Kishida, K. Araki, S. Kishiba and K. Suzuki,
Local or Nonlocal? Orthonormal Divergence-free Wavelet Analysis of Nonlinear Interactions in Turbulence Mar. 1999

NIFS-590 K. Araki, K Suzuki, K. Kishida and S. Kishiba,
Multiresolution Approximation of the Vector Fields on T^3; Mar. 1999

NIFS-591 K. Yamazaki, H. Yamada, K.Y.Watanabe, K. Nishimura, S. Yamaguchi, H. Nakanishi, A. Komori, H Suzuki, T. Mito, H. Chikaraishi, K Murai, O Motojima and the LHD Group,
Overview of the Large Helical Device (LHD) Control System and Its First Operation Apr 1999

NIFS-592 T. Takahashi and Y. Nakao,
Thermonuclear Reactivity of D-T Fusion Plasma with Spin-Polarized Fuel, Apr 1999

NIFS-593 H. Sugama,
Damping of Toroidal Ion Temperature Gradient Modes: Apr 1999

NIFS-594 Xiaodong Li,
Analysis of Crowbar Action of High Voltage DC Power Supply in the LHD ICRF System, Apr 1999

NIFS-595 K Nishimura, R Horiuchi and T Sato,
Drift-kink Instability Induced by Beam Ions in Field-reversed Configurations, Apr 1999

NIFS-596 Y. Suzuki, T-H Watanabe, T. Sato and T Hayashi,
Three-dimensional Simulation Study of Compact Toroid Plasmoid Injection into Magnetized Plasmas; Apr. 1999

NIFS-597 H. Sanuki, K. Itoh, M Yokoyama, A. Fujisawa, K. Ida, S Toda, S.-I Itoh, M Yagi and A. Fukuyama,
Possibility of Internal Transport Barrier Formation and Electric Field Bifurcation in LHD Plasma,
May 1999

NIFS-598 S. Nakazawa, N. Nakajima, M. Okamoto and N. Ohyabu,
One Dimensional Simulation on Stability of Detached Plasma in a Tokamak Divertor: June 1999